

Effects of arterial geometry on aneurysm growth: three-dimensional computational fluid dynamics study

YIEMENG HOI, M.S., HUI MENG, PH.D., SCOTT H. WOODWARD, M.S.,
BERNARD R. BENDOK, M.D., RICARDO A. HANEL, M.D.,
LEE R. GUTERMAN, PH.D., M.D., AND L. NELSON HOPKINS, M.D.

Department of Mechanical and Aerospace Engineering, Department of Neurosurgery, Toshiba Stroke Research Center, School of Medicine and Biomedical Sciences, University at Buffalo, The State University of New York, Buffalo, New York; and Department of Neurological Surgery, Northwestern University, Chicago, Illinois

Object. Few researchers have quantified the role of arterial geometry in the pathogenesis of saccular cerebral aneurysms. The authors investigated the effects of parent artery geometry on aneurysm hemodynamics and assessed the implications relative to aneurysm growth and treatment effectiveness.

Methods. The hemodynamics of three-dimensional saccular aneurysms arising from the lateral wall of arteries with varying arterial curves (starting with a straight vessel model) and neck sizes were studied using a computational fluid dynamics analysis. The effects of these geometric parameters on hemodynamic parameters, including flow velocity, aneurysm wall shear stress (WSS), and area of elevated WSS during the cardiac cycle (time-dependent impact zone), were quantified. Unlike simulations involving aneurysms located on straight arteries, blood flow inertia (centrifugal effects) rather than viscous diffusion was the predominant force driving blood into aneurysm sacs on curved arteries. As the degree of arterial curvature increased, flow impingement on the distal side of the neck intensified, leading to elevations in the WSS and enlargement of the impact zone at the distal side of the aneurysm neck.

Conclusions. Based on these simulations the authors postulate that lateral saccular aneurysms located on more curved arteries are subjected to higher hemodynamic stresses. Saccular aneurysms with wider necks have larger impact zones. The large impact zone at the distal side of the aneurysm neck correlates well with other findings, implicating this zone as the most likely site of aneurysm growth or regrowth of treated lesions. To protect against high hemodynamic stresses, protection of the distal side of the aneurysm neck from flow impingement is critical.

KEY WORDS • aneurysm • cerebrovascular circulation • hemodynamics •
arterial remodeling • stroke • endovascular therapy

STROKE is the third leading cause of death in the US. Subarachnoid hemorrhage accounts for approximately 7% of stroke cases and the majority of these cases are caused by rupture of a cerebral aneurysm.²⁸ Approximately 50% of patients with aneurysmal SAH will die or suffer severe disability as a result of the initial hemorrhage; another 23 to 35% will die as a result of subsequent hemorrhage if the aneurysm is not treated.¹³

The pathogenesis of cerebral aneurysms is significantly influenced by the local hemodynamic environment; successful treatment must favorably modify this environment to promote thrombotic aneurysm occlusion and healthy arterial remodeling. It has been observed clinically that most cerebral aneurysms arise from areas subjected to increased hemodynamic forces, that is, at the apex of arterial bifurcations or on the curve of tortuous vessels (Fig. 1), rather than along straight vessel segments.²⁷ Geometric parameters, such as aneurysm volume, shape, aspect ratio, and dome-to-neck ratio, have been studied extensively;^{9,15,25,35} however, little information characterizing the relation of the local vessel and aneurysm geometry to these elevated hemodynamic forces is available.^{6,19,24}

Abbreviations used in this paper: CFD = computational fluid dynamics; WSS = wall shear stress; 3D = three-dimensional.

In this study we begin the process of quantifying the poorly understood hemodynamic effects resulting from the complex 3D geometry of the local vessel. The first step undertaken was to quantify the relationship between hemodynamic forces and arterial curvature in an attempt to establish further correlations for the effect of arterial geometry on aneurysm growth and treatment.

Computational fluid dynamics is a computer simulation method that can be used to model the complex in vivo flow field associated with cerebral aneurysms. A time-dependent, space-resolved, 3D flow velocity field in anatomically realistic cerebral aneurysm models can be obtained from CFD simulations. Using the flexibility of CFD, the parameters of fluid dynamics and the blood particle paths can then be directly calculated and visualized. Furthermore, CFD can be used to predict the success or failure of interventional therapies that rely on altering the dynamics of blood flow within the aneurysm sac.

A better understanding of the relationship between the pathophysiological aspects of an aneurysm and its arterial geometry or local hemodynamics is critical to understanding aneurysm growth, predicting the risk of regrowth after treatment, and improving endovascular treatments. Our objective in this study was to examine the effects of local vessel curvature and aneurysm neck size on the hemodynamics

Effects of arterial geometry on aneurysm growth

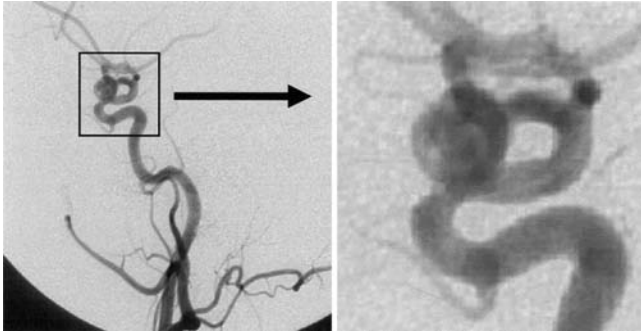


FIG. 1. Conventional digital subtraction angiograms demonstrating a typical saccular cerebral aneurysm arising from the lateral wall of a curved parent artery (enlarged view on right).

of an aneurysm and, using a CFD analysis, to correlate these parameters with aneurysm growth and potential treatment effectiveness.

Materials and Methods

We analyzed 3D saccular (spherical) aneurysm models with varying arterial curvatures and aneurysm neck sizes to quantify the role of local hemodynamic forces within the aneurysm. To isolate the arterial curvature and aneurysm neck size from numerous other geometric and physiological factors present in human aneurysms, we adopted anatomically realistic aneurysm geometries in which we could systematically vary the curvature of the parent vessel and the aneurysm neck while keeping other parameters unchanged.

Geometric Parameters

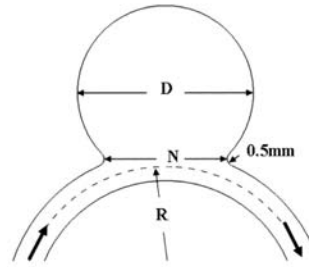
The following definitions for geometric variables of interest were used for each model: R, radius of the curvature of the parent artery; $1/R$, curvature of the parent artery (the inverse of R); D, diameter of the aneurysm; N, width (major axis) of the aneurysm neck; and d, the internal diameter of the parent artery (Fig. 2). In the first group of models, denoted R1 through R6, the geometric variables were kept constant, except for the parent artery curvature ($1/R$). In the second group of models, denoted N1 through N4, the geometric variables were kept constant, except for the aneurysm neck size (N). In all 10 models, the parent artery was 3 mm in diameter and the aneurysm was 12 mm in diameter. In the first group, the curvature of the parent artery ranged from 0 (a straight vessel) to 0.167 mm^{-1} and the width of the aneurysm neck was kept at 7.5 mm. In the second group, the width of the neck ranged from 6 to 9.56 mm, and the curvature of the parent artery was fixed at 0.083 mm^{-1} .

Computational Tools

The computational mesh consisted of a 3D hybrid tetrahedral and hexagonal mesh generated using Gambit software (Fluent, Inc., Lebanon, NH). Each 3D model consisted of approximately 500,000 cells. The finite-volume commercial code STARCD (CD Adapco, Melville, NY) was used to simulate 3D blood flow.

Flow Model

Consistent with established approaches to CFD in large arteries,^{1,26} we assumed incompressible, laminar flow in a rigid model and conducted simulations using a finite-volume algorithm in a 3D domain. Based on the Reynolds number, the flow was found to be well within the laminar regime, unlike that found closer to the heart or in some constricted vessels. In large vessels ($> 0.5 \text{ mm}$) with very low shear rates, like those in our models, nonnewtonian effects in blood flow are regarded as second order and consequently neglected;^{1,3,23} therefore, the blood was modeled as a newtonian fluid with a viscosity (μ) of 3.5 cP and a density (ρ) of 1060 kg/m^3 . The computational domain of the vessel was extended to ensure zero-velocity gradients at the outlet. A no-slip condition was applied to all walls. The rigid wall as-



| Model | $1/R(\text{mm}^{-1})$ | N (mm) |
|-----------|-----------------------|--------|
| R1 | 0.000 | 7.500 |
| R2 | 0.067 | 7.500 |
| R3 | 0.083 | 7.500 |
| R4 | 0.100 | 7.500 |
| R5 | 0.125 | 7.500 |
| R6 | 0.167 | 7.500 |
| N1 | 0.083 | 6.000 |
| N2 | 0.083 | 6.085 |
| N3 | 0.083 | 8.000 |
| N4 | 0.083 | 9.560 |
| D = 12 mm | | |
| d = 3 mm | | |

FIG. 2. Geometric representation of an aneurysm located on a curved parent artery. Two groups of aneurysm models are represented: R1 through R6 and N1 through N4. In the R models the degree of the parent artery curvature is varied, whereas in the N models the size of the aneurysm orifice is varied. Arrows indicate the direction of blood flow (or of inflow and outflow). D = diameter of the aneurysm; d = internal diameter of the parent artery; N = width (major axis) of the aneurysm neck; $1/R$ = curvature of the parent artery.

sumption was used to simplify the computation. A distensible aneurysm wall will further increase blood flow into the aneurysm and has been found to increase the magnitude of the WSS in the impact zone approximately 8%.²⁰ The size and magnitude of the WSS impact zone should be considered by erring on the conservative side.

We conducted steady-state and pulsatile flow simulations in 10 aneurysm models. In the steady-state flow simulations, two parabolic velocity profiles with constant maximal velocities (U) of 59.7 cm/second and 30 cm/second, respectively, were assumed at the inlet. The corresponding Reynolds numbers ($Re = \rho U d / \mu$), which indicate the relative magnitude of inertia as opposed to the viscous force of the flow, were approximately 136 and 270, respectively. In the pulsatile flow simulations, a velocity waveform that matched a physiological cerebral waveform was constructed using four terms of its Fourier series. For these simulations, the Reynolds numbers at the maximal, minimal, and mean rates of flow were approximately 270, 37, and 136, respectively. The Womersley number, which is used to measure the ratio of transient inertia from pulsatility over viscous force, was approximately 2.07 in the pulsatile flow simulations.

Hemodynamic Variables

It is widely accepted that arteries adapt to changes in blood flow conditions through remodeling. Wall shear stress is the tangential force exerted by flowing blood on the luminal surface that retards the flow of blood. The endothelial cells detect mechanical strain caused by the WSS and respond to this strain by adjusting the vessel diameter to restore the WSS to a baseline level of 15 to 20 dynes/cm².^{16,18,21,34} This biological response is accomplished primarily by the release of vasodilators that allow smooth-muscle cells to relax, ultimately causing the vessels to dilate.^{16,18,34} Building on this premise, we calculated the area of the aneurysm wall where the WSS was elevated and greater than 20 dynes/cm². This elevated WSS area may indicate the site of active remodeling of the aneurysm wall. We defined this area as the impact zone. The time-dependent, space-resolved, 3D flow-velocity field, the WSS, and the impact zone in each 3D model were obtained from these simulations. We computed the blood flow velocity and the WSS distribution for all aneurysm models through both steady-state and pulsatile flow simulations. In the pulsatile flow simulations, time-dependent WSS distributions were also computed to quantify the impact zone.

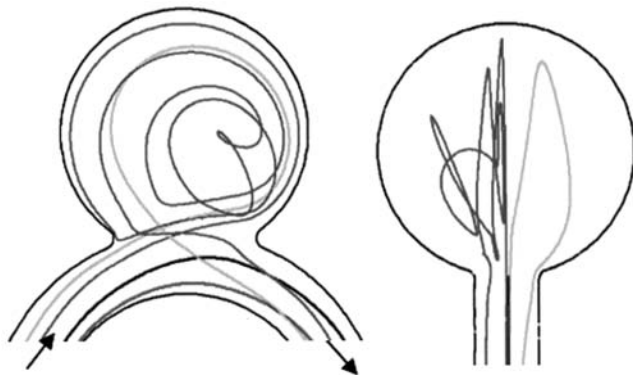


FIG. 3. Drawing showing the results of the simulation of blood-particle paths in model R5 at a steady state. Some blood paths never enter the aneurysm, whereas others enter it from the distal side of the neck. Of those paths entering the aneurysm, some leave at the distal side of the neck, whereas others join the inflow and whirl irregularly inside the lesion. The paths flow from left to right (left) and off the paper, toward the reader (right).

Results

Unless otherwise noted, only results from pulsatile flow simulations are presented in this paper.

Aneurysm flow is a highly complex 3D phenomenon. The flow dynamics were visualized by tracking the paths of blood particles. We traced a group of uniformly distributed blood-particle paths from the inlet boundary of the computational domain (Fig. 3). Some of the paths never entered the aneurysm. All paths that entered the aneurysm did so near the distal side of the neck in all models. Of those paths entering the aneurysm, some left at the proximal side of the neck with a lower velocity, whereas others joined the inflow from the parent artery, entered the cavity again, and whirled irregularly within the aneurysm.

Flow impingement intensified with increasing curvature. Figure 4 shows snapshots of flow velocity vectors at the symmetry plane, which were captured at maximum systole in models with different curvatures. When the curvature was insignificant or even zero (as in the case of the straight vessel model R1), the vorticity at the distal side of the neck

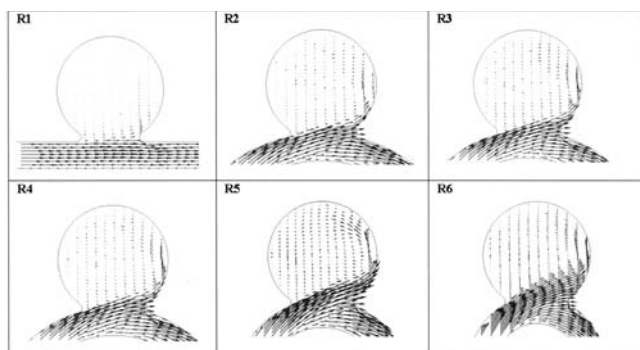


FIG. 4. Comparative drawings of the velocity field at the symmetry plane in different models at maximum systole. The curvature increases from 0 (straight vessel) in model R1 to 0.167 mm^{-1} in model R6. As the degree of arterial curvature increases, the flow impingement on the distal side of the aneurysm neck intensifies.

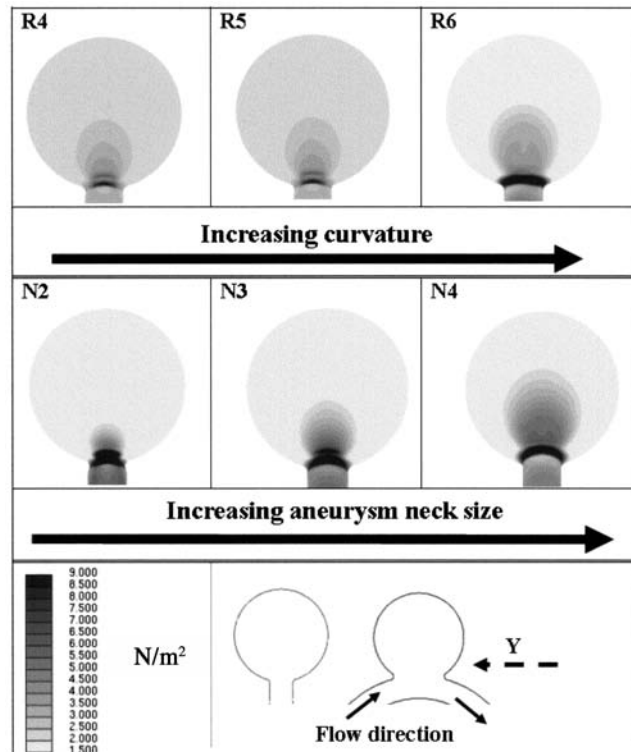


FIG. 5. Photographs and drawings showing the WSS distribution at the distal side of the neck in models R4, R5, R6, N2, N3, and N4 at maximum systole during the pulsatile flow simulations. The figures shown here are viewed from the Y direction (see lower diagram), looking at the distal side of the aneurysm dome and neck.

weakly entrained the flow into the aneurysm. In arteries with more pronounced curvature (as in the case of curved model R6), the velocity profiles were skewed toward the outer wall of the lesion, indicating the effect of centrifugal force in all models. Blood flow entered the aneurysm from the distal side of the neck and was primarily driven by the inertia of the blood. As the result of increases in the degree of arterial curvature or the major axis of the aneurysm orifice (neck), a larger volume of higher-momentum blood was observed to impinge more strongly on the distal side of the aneurysm neck. The high-momentum blood formed a strong vortex in the aneurysm cavity; the distal side of the neck can be thought of as a flow divider.

The impact zone enlarged with increases in arterial curvature and the size of the aneurysm neck. Figure 5 shows that flow impingement led to an elevation in the WSS at the distal side of the neck, as a result of increasing either the degree of arterial curvature or the size of the neck. It is clear that the aneurysm dome does not have a uniform WSS distribution. The area on the aneurysm wall at which the WSS became elevated—the impact zone—increased in size with stronger flow impingement. This increase appears to be a function of arterial curvature or aneurysm neck size or both. To quantify this relationship, we plotted the impact zone as a function of arterial curvature or aneurysm neck size or both. Figure 6 shows the relationship between the impact zone at peak systole and the geometric variable $N3/R$. The impact zone was observed to increase linearly with parent artery curvature ($1/R$) and the third order of aneurysm neck

Effects of arterial geometry on aneurysm growth

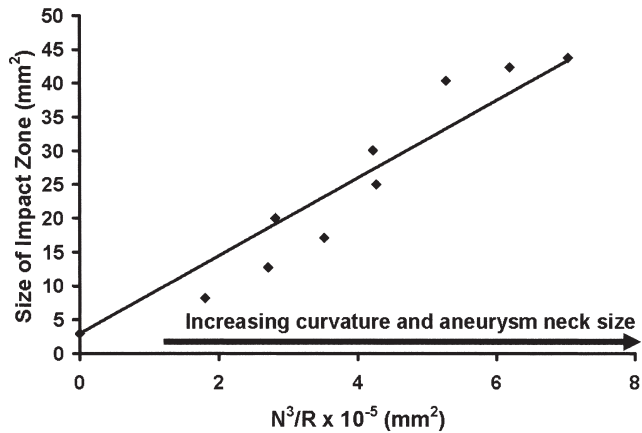


FIG. 6. Graph demonstrating that the impact zone at peak systole is a function of aneurysm neck size (N) and curvature (1/R). A larger aneurysm neck size on a more curved artery may promote artery remodeling and an increased likelihood of aneurysm growth.

size (N). Figure 7 shows the relationship of the impact zone and the parent artery curvature at different Reynolds numbers. In our simulations, higher flow rates resulted in the intensification of flow impingement on the aneurysm wall, thus generating a larger impact zone.

The impact zone at the distal side of the aneurysm neck changed dynamically during the cardiac cycle and enlarged with increasing arterial curvature (Fig. 8). The more curved the vessel, the larger the impact zone.

Discussion

Influence of an Elevated WSS on Aneurysm Dilatation

Our simulations have shown that flow impingement elevates both pressure and WSS at the distal side of the neck of a saccular aneurysm arising from the lateral wall of a curved artery. As previously mentioned, endothelial cells at the flow impingement zone respond to elevated WSS by releasing vasodilation factors to remodel the wall in an attempt to return the WSS to the baseline levels of 15 to 20 dynes/cm².^{16,18,21,34} These factors, including nitric oxide, prostacyclin (PGI₂), and matrix metalloproteinases, degrade the extracellular matrix and dilate the arterial wall by relaxing smooth-muscle cells at the flow impingement zone.^{18,31,33} The absence or disorganization of key extracellular matrix components, mainly collagen and elastin, decrease the mechanical strength of the aneurysm wall. In addition, the elevated pulsatile pressure plays a role in stretching and expanding the aneurysm wall from the distal side of the neck. The weakened wall, in conjunction with the stretching caused by this pressure, becomes more susceptible to dilation.^{4,14} Furthermore, as the wall continues to degrade and be stretched from the distal neck, healthier portions of the parent artery become incorporated into the aneurysm. As a result, the aneurysm enlarges, continuously experiences flow impingement, and undergoes further degradation and stretching. Our findings are in agreement with the theory that intense flow impingement induces degeneration of arterial wall components, leading to aneurysm dilation.^{4,29,35}

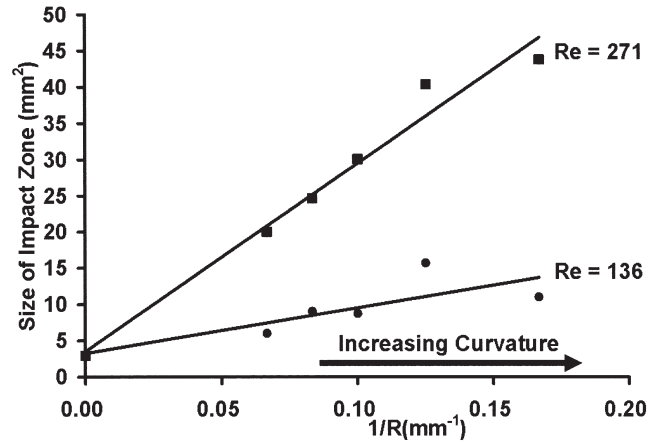


FIG. 7. Graph showing that with increasing curvature of the vessel, the impact zone size increases almost linearly. Higher degrees of arterial curvature or higher rates of flow may induce more active arterial remodeling and promote aneurysm growth.

Risk of Aneurysm Growth Increases With Larger Arterial Curvature and Aneurysm Neck Size

Our simulations have shown that as the degree of parent vessel curvature or the size of the aneurysm neck increases, flow impingement intensifies, leading to an increase in the impact zone (Fig. 8). It is reasonable to expect that with an increasing impact zone, the quantity of vascular remodeling factors that is released also increases accordingly. In an attempt to restore the elevated WSS to the baseline level, the increase in the quantity of vascular remodeling factors leads to a more rapid remodeling process, as mentioned earlier. Ultimately, these remodeling factors will lead to a higher likelihood of wall injury and aneurysm growth.^{11,12,30} Therefore, we postulate that aneurysms with large necks and those located on vessels with high degrees of curvature are susceptible to greater risks of continuous growth. Furthermore, that the impact zone varies in a linear fashion

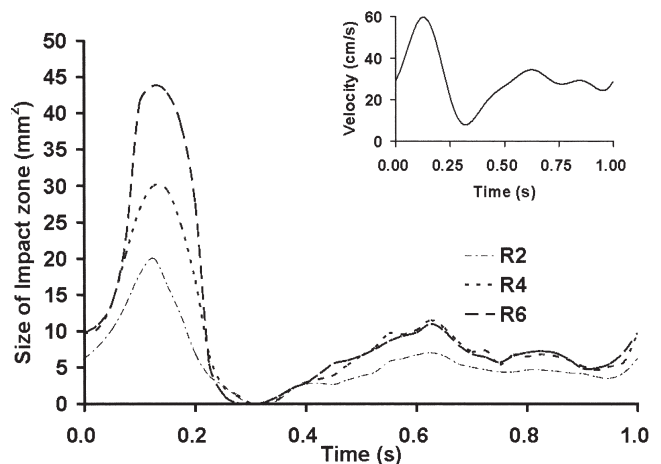


FIG. 8. Graph demonstrating that the size of the impact zone at the distal neck varied dynamically during a cardiac cycle. This variation is more pronounced with increasing arterial curvature in models R2, R4, and R6. The smaller graph (*inset*) shows the velocity profile over a cardiac cycle in a pulsatile flow simulation.

with arterial curvature but in a cubical fashion with neck size indicates that neck size has a stronger effect than arterial curvature on the risk of aneurysm growth.

Our work indicates that aneurysms on vessels with a high degree of curvature may grow at a faster rate than their counterparts on straight vessels. Based on our simulations we posit that asymptomatic aneurysms with large necks or aneurysms located on vessels with a great degree of curvature may require intervention at an earlier stage than other aneurysms.

Therapies Developed for Aneurysms on Straight Vessels May Not Be Effective for Those on Curved Vessels

The introduction of vascular stents to aid in coil embolization has opened the door to the thrombotic occlusion of aneurysms through stent placement. Geremia and colleagues^{7,8} and Wakhloo, et al.,³⁶ have demonstrated complete occlusion of sidewall and fusiform aneurysms on the carotid arteries of dogs by using stents alone. A drawback of these studies is that they are limited to aneurysms located on straight vessels, an anatomical configuration that is seldom encountered clinically.

We believe that as a result of significantly different flow mechanisms, saccular aneurysms located on curved vessels are less apt to thrombose than their counterparts on straight vessels. For a saccular aneurysm located on a straight vessel, blood flow entering the aneurysm is predominantly driven by viscous shear force. The vorticity at the proximal aneurysm neck weakly entrains flow into the aneurysm. Consequently, a low-momentum flow entering a lateral aneurysm that is located on a straight vessel or one with a small degree of curvature creates a more stasislike environment, increasing the likelihood of thrombosis,¹⁹ which in turn increases the likelihood for successful treatment. On the other hand, in an aneurysm located on a curved vessel, the inertia of the blood flow (centrifugal effect) must be overcome by the artery wall to make the blood travel along the curve. This inertia-driven mechanism produces a stronger impingement of flow on the distal side of the aneurysm neck and generates a coherent vortex within the lesion. In a lateral aneurysm located on a vessel with a high degree of arterial curvature, blood is continuously refreshed and the length of time that blood resides in the aneurysm sac is reduced. This increase in blood circulation in aneurysms located on more tortuous vessels may lead to a reduced likelihood to form a stable thrombus. This type of aneurysm may also be associated with a greater risk of growth and should therefore be examined with greater care.

Although bridging the aneurysm neck with a stent may sufficiently alter blood flow in an aneurysm located on a straight vessel and thus induce a thrombotic occlusion,^{7,8,35} a stent alone may not provide durable treatment for an aneurysm on a curved vessel. The standard high-porosity stent may not sufficiently dampen the inertia of the flow impingement to create the prothrombotic environment necessary for aneurysm occlusion. It has been observed, however, that the stent may straighten the vessel to some degree³⁷ and would therefore reduce the WSS at the distal side of the aneurysm neck. We speculate that bridging the neck with only the type of stent that is currently commercially available should positively alter the blood flow and slow aneurysm growth, but it will most likely not be ade-

quate to induce complete occlusion in an aneurysm on a curved vessel.

Effectiveness of Endovascular Treatment and Aneurysm Geometry

As a result of intense flow impingement and observed growth at the distal side of the aneurysm neck, a high degree of arterial curvature and a large neck size may decrease the effectiveness of endovascular treatment of cerebral aneurysms. Endovascular coil embolization has been promoted as a less invasive therapeutic alternative to surgical clip placement for the occlusion of cerebral aneurysms from the circulation.²² Loose coil packing together with exposure of the aneurysm neck to flow, however, has been known to lead to incomplete occlusion in the majority of wide-necked aneurysms.^{5,10} Our findings indicate that flow impingement, which is implicated especially in conjunction with a high degree of arterial curvature and large aneurysm neck size, is ultimately responsible for compacting the coils. The incessant oscillating inertia of the pulsatile flow pushes the coils and localized adherent thrombi toward the aneurysm dome, exposing the distal neck; this results in the continued exposure to an elevated WSS and the increased likelihood for regrowth of a treated aneurysm.^{10,17} Dilation of the aneurysm wall at the distal side of the neck results in the incorporation of an increasing amount of normal parent vessel wall into the aneurysm. Hence, coil-treated aneurysms that are located on an arterial segment with a high degree of curvature or that have large neck sizes may be at great risk of regrowth. A correlation with clinical observations will be needed to quantify this relationship.

Successful occlusion of an aneurysm and prevention of its regrowth depend on protection of the impact zone. To increase the durability of endovascular aneurysm treatment, interventions should be aimed at protecting the aneurysm wall from flow impingement, sufficiently dampening the momentum of blood entering the aneurysm, and creating a prothrombotic environment. These recommendations may likewise be applied to bifurcation aneurysms, but the geometric variability is so great in such cases that the location of the impact zone cannot be so easily generalized to the distal side of the neck.

Conclusions

Analysis of our 3D CFD studies, in which minor alterations in local anatomical geometric parameters and the local hemodynamic environment were made, indicates that a greater chance of aneurysm growth on a high degree of arterial curvature exists if the inflow momentum is not impeded. A large impact zone on the aneurysm wall appears to be the most likely site for aneurysm initiation and for growth or regrowth of a treated aneurysm. An aneurysm with a wide neck located on a curved vessel should be accessed with a heightened awareness of its increased hemodynamic stresses. To occlude an aneurysm successfully and to prevent its regrowth, it is essential that the impact zone be protected.

Our analysis has shown that hemodynamic stresses are time dependent—varying greatly over the cardiac cycle—and location dependent—varying significantly throughout the aneurysm. The local hemodynamics of an aneurysm

Effects of arterial geometry on aneurysm growth

will affect the progression of aneurysm growth and the effectiveness of endovascular treatments. The integration of CFD simulations with medical diagnostic imaging techniques has provided new insights to assess the pathogenesis of an aneurysm on an individual basis.^{2,32} This integrated methodology may advance our knowledge of aneurysm hemodynamics, predict the outcome of surgical procedures, and help us assess specific risks to individual patients.

Acknowledgments

We thank Balazs Nemes, M.D., Stephen Rudin, Ph.D., and Kenneth Hoffmann, Ph.D., for helpful discussions and critiques of this manuscript.

References

1. Burlison AC, Strother CM, Turitto VT: Computer modeling of intracranial saccular and lateral aneurysms for the study of their hemodynamics. **Neurosurgery** **37**:774–784, 1995
2. Cebal JR, Löhner R: From medical images to anatomically accurate finite element grids. **Int J Num Meth Eng** **51**:985–1008, 2001
3. Dutta A, Tarbell JM: Influence of non-Newtonian behavior of blood on flow in an elastic artery model. **J Biomech Eng** **118**:111–119, 1996
4. Ferguson GG: Physical factors in the initiation, growth, and rupture of human intracranial saccular aneurysms. **J Neurosurg** **37**:666–677, 1972
5. Fernandez Zubillaga A, Guglielmi G, Viñuela F, et al: Endovascular occlusion of intracranial aneurysms with electrically detachable coils: correlation of aneurysm neck size and treatment results. **AJNR** **15**:815–820, 1994
6. Foutarakis GN, Yonas H, Sclabassi RJ: Saccular aneurysm formation in curved and bifurcating arteries. **AJNR** **20**:1309–1317, 1999
7. Geremia G, Brack T, Brennecke L, et al: Occlusion of experimentally created fusiform aneurysms with porous metallic stents. **AJNR** **21**:739–745, 2000
8. Geremia G, Haklin M, Brennecke L: Embolization of experimentally created aneurysms with intravascular stent devices. **AJNR** **15**:1223–1231, 1994
9. Gonzalez CF, Cho YI, Ortega HV, et al: Intracranial aneurysms: flow analysis of their origin and progression. **AJNR** **13**:181–188, 1992
10. Graves VB, Strother CM, Partington CR, et al: Flow dynamics of lateral carotid artery aneurysms and their effects on coils and balloons: an experimental study in dogs. **AJNR** **13**:189–196, 1992
11. Guzman RJ, Abe K, Zarins CK: Flow-induced arterial enlargement is inhibited by suppression of nitric oxide synthase activity in vivo. **Surgery** **122**:273–280, 1997
12. Hademenos GJ, Massoud TF: Biophysical mechanisms of stroke. **Stroke** **28**:2067–2077, 1997
13. Heros RC, Kistler JP: Intracranial arterial aneurysm—an update. **Stroke** **14**:628–631, 1983
14. Imbesi SG, Kerber CW: Analysis of slipstream flow in a wide-necked basilar artery aneurysm: evaluation of potential treatment regimens. **AJNR** **22**:721–724, 2001
15. Kassell NF, Torner JC: Size of intracranial aneurysms. **Neurosurgery** **12**:291–297, 1983
16. Ku DN: Blood flow in arteries. **Ann Rev Fluid Mechanics** **29**:399–434, 1997
17. Kwan ES, Heilman CB, Shucart WA, et al: Enlargement of basilar artery aneurysms following balloon occlusion—“water-hammer effect.” Report of two cases. **J Neurosurg** **75**:963–968, 1991
18. Lehoux S, Tronc F, Tedgui A: Mechanisms of blood flow-induced vascular enlargement. **Biorheology** **39**:319–324, 2002
19. Liou TM, Liao CC: Flowfields in lateral aneurysm models arising from parent vessels with different curvatures using PTV. **Exp Fluids** **23**:288–298, 1997
20. Low M, Perktold K, Raunig R: Hemodynamics in rigid and distensible saccular aneurysms: a numerical study of pulsatile flow characteristics. **Biorheology** **30**:287–298, 1993
21. Malek AM, Alper SL, Izumo S: Hemodynamic shear stress and its role in atherosclerosis. **JAMA** **282**:2035–2042, 1999
22. Murayama Y, Song JK, Uda K, et al: Combined endovascular treatment for both intracranial aneurysm and symptomatic vasospasm. **AJNR** **24**:133–139, 2003
23. Nichols WW, O’Rourke MF: **McDonald’s Blood Flow in Arteries—Theoretical, Experimental and Clinical Principles**, ed 4. New York: Oxford University Press, 1999
24. Niimi H, Kawano Y, Sugiyama I: Structure of blood flow through a curved vessel with an aneurysm. **Biorheology** **21**:603–615, 1984
25. Parlea L, Fahrig R, Holdsworth DW, et al: An analysis of the geometry of saccular intracranial aneurysms. **AJNR** **20**:1079–1089, 1999
26. Perktold K, Peter R, Resch M: Pulsatile non-Newtonian blood flow simulation through a bifurcation with an aneurysm. **Biorheology** **26**:1011–1030, 1989
27. Rhoton AL Jr: Aneurysms. **Neurosurgery** **51** (Suppl 4):S121–S158, 2002
28. Ronkainen A, Hernesniemi J, Puranen M, et al: Familial intracranial aneurysms. **Lancet** **349**:380–384, 1997
29. Sekhar LN, Heros RC: Origin, growth, and rupture of saccular aneurysms: a review. **Neurosurgery** **8**:248–260, 1981
30. Stehbens WE: Flow disturbances in glass models of aneurysms at low Reynolds numbers. **Q J Exp Physiol Cogn Med Sci** **59**:167–174, 1974
31. Steiger HJ: Pathophysiology of development and rupture of cerebral aneurysms. **Acta Neurochir Suppl** **48**:1–57, 1990
32. Steinman DA, Milner JS, Norley CJ, et al: Image-based computational simulation of flow dynamics in a giant intracranial aneurysm. **AJNR** **24**:559–566, 2003
33. Szikora I, Wakhloo AK, Guterman LR, et al: Initial experience with collagen-filled Guglielmi detachable coils for endovascular treatment of experimental aneurysms. **AJNR** **18**:667–672, 1997
34. Tronc F, Mallat Z, Lehoux S, et al: Role of matrix metalloproteinases in blood flow-induced arterial enlargement: interaction with NO. **Arterioscler Thromb Vasc Biol** **20**:E120–E126, 2000
35. Ujiie H, Tamano Y, Sasaki K, et al: Is the aspect ratio a reliable index for predicting the rupture of a saccular aneurysm? **Neurosurgery** **48**:495–503, 2001
36. Wakhloo AK, Lanzino G, Lieber BB, et al: Stents for intracranial aneurysm: the beginning of a new endovascular era? **Neurosurgery** **43**:377–379, 1998
37. Wentzel JJ, Whelan DM, van der Giessen WJ, et al: Coronary stent implantation changes 3-d vessel geometry and 3-d shear stress distribution. **J Biomech** **33**:1287–1295, 2000

Manuscript received December 1, 2003.

Accepted in final form June 9, 2004.

This study was supported by grants from Toshiba America, the Oishei Foundation, and the Cummings Foundation (L.N.H.)

Address reprint requests to: Hui Meng, Ph.D., Department of Mechanical and Aerospace Engineering, University at Buffalo, The State University of New York, 324 Jarvis Hall, Buffalo, New York 14620. email: huimeng@buffalo.edu.